Journal of Solid State Chemistry 183 (2010) 344–349

Contents lists available at ScienceDirect

Journal of Solid State Chemistry

journal homepage: www.elsevier.com/locate/jssc

Spin-driven ferroelectricity in the delafossite $CuFe_{1-x}Rh_xO_2$ ($0 \le x \le 0.15$)

E. Pachoud *, C. Martin, B. Kundys [1], Ch. Simon, A. Maignan

Laboratoire CRISMAT, UMR 6508 CNRS/ENSICAEN, 6 bd du Maréchal Juin, F-14050 CAEN Cedex 4, France

ARTICLE INFO

Article history:
Received 10 August 2009
Received in revised form
6 November 2009
Accepted 21 November 2009
Available online 2 December 2009

Keywords:
Oxide
Delafossite
Polarisation
Magnetic properties
Multiferroic materials

ABSTRACT

The effect of substitution at the Fe site in the $CuFeO_2$ delafossite is known to induce a magnetic structure responsible for the appearance of electric polarization. A $CuFe_{1-x}Rh_xO_2$ series of ceramic samples is studied in order to determine the composition range exhibiting such a polar state. It is found that for the $CuFe_{1-x}Rh_xO_2$ ($x \le 0.15$) solid solution, the Néel temperature T_{N2} decreases monotonously with x from 11.5 K to 5.9 K, for x=0.00 to 0.15, respectively, and that the dielectric peak and the polarization transition temperatures coincide with T_{N2}. In contrast, the dielectric peak and polarization magnitudes go through an optimum for $CuFe_{0.92}Rh_{0.08}O_2$ (x=0.08). These results demonstrate that, compared to other substituting elements, the Rh^{3+} for Fe^{3+} substitution in $CuFeO_2$ allows to extend significantly the ferroelectric region in the (x, T) phase diagram in connection with the slower T_{N2} decrease.

1. Introduction

In transition metal oxides, substitutions at the metal site are known to be a powerful technique to modify the background physical properties as charge/spin/orbital ordering. Well documented examples have been reported for Fe_3O_4, Ti_4O_7 [1] or for $Pr_{0.5}Ca_{0.5}MnO_3$ half-doped manganites [2]. More recently, such substitutions in multiferroic oxides have been shown to induce magneto-electric effects (electric polarization to spins coupling or vice-versa) associated to a non-collinear (spiral) antiferromagnetic state: for instance, in the delafossite $CuFeO_2$, magnetic fields H of several teslas are required to induce the first transition to a polar phase [3,4], whereas in $CuFe_{1-x}Al_xO_2$, the Al^{3+} substitution in the range $0.014 \le x \le 0.030$ creates a similar ferroelectric state without applied magnetic field [5–7]. Such substitutions transform the collinear commensurate four-sublattice structure of $CuFeO_2$ to a ferroelectric proper helical structure in $CuFe_{1-x}Al_xO_2$, i.e. act as the application of an external magnetic field [5–9]. Other effects are also induced by substitutions in delafossite oxides as in $CuRhO_2$. For instance, the electronic ground state of $CuRhO_2$ evolves from insulator to metallic as 10% Mg^{2+} is substituted for rhodium [10].

Coming back to the $CuFeO_2$ delafossite, other trivalent doping elements for Fe such as Ga^{3+} [11] and Rh^{3+} [12], have been also reported to be efficient to induce a ferroelectric state. This effect is reported for a larger substitution level for Rh (i.e. 5%) in a polycrystalline sample than in the Al^{3+} or Ga^{3+} substituted single crystals. This has motivated us to investigate in $CuFeO_2$ the role of the Rh^{3+} amount upon the electric state and magnetic properties. Furthermore, this system is worth studying as it appears recently that electric polarization may exist irrespectively of the spin chirality propagation direction in $DyMnO_3$ [13], $CuFe_{1-x}Al_xO_2$ [8] and $CuCrO_2$ [14]. This suggests that the spin–current model [15] is not always working for spin driven electric polarization. In fact, the proper helical structure observed in the ferroelectric incommensurate phase of $CuFe_{1-x}Al_xO_2$ by neutron diffraction strongly suggests correlation between spin non-collinearity and ferroelectricity [16]. Furthermore, as magnetic field induced switching of the electric polarization from one crystallographic direction to another has been reported in rare earth manganites [17,18] and in $MnWO_4$ [19–21], one has to anticipate possible direction changes of electric polarization upon T and/or H changes. For this reason, polarization measurements of polycrystalline samples with isotropic distribution of the microcrystals are useful to investigate new systems as they allow averaging all directions. Spin-driven polarization has been recently reported for polycrystals of $CuCrO_2$ [14], $YBaCuFeO_5$ [22] and $CuFe_{0.95}Rh_{0.05}O_2$ [12].

In the following, we report on the preparation, structural characterizations and physical properties—magnetic and magneto(di)electric—of several polycrystalline compounds belonging to the delafossite $CuFe_{1-x}Rh_xO_2$ series. It is found that this isoelectronic substitution, although keeping almost unchanged the room temperature rhombohedral unit cell and the first Néel temperature T_{N1}, induces a monotonous T_{N2} decrease from T_{N2}=11.5 to 5.9 K as x increases from x=0.00 to 0.15, respectively. Contrasting to this T_{N2} linear dependence with x, the induced polarization

* Corresponding author. Fax: +33 2 31 95 16 00.
E-mail address: elise.pachoud@ensicaen.fr (E. Pachoud).
[1] Present address: Service de Physique de l'Etat Condensé, DSM/DRECAM, CEA Saclay, 91191 Gif-Sur-Yvette Cedex, France.

0022-4596/$ - see front matter © 2009 Elsevier Inc. All rights reserved.
doi:10.1016/j.jssc.2009.11.023

value in zero magnetic field is found to go through a maximum for x=0.08, reaching 110 μC/cm^2 at 6 K. The evidence for existence of the electric polarization in a much broader range of substitution as compared to the $CuFe_{1-x}Al_xO_2$ series suggests that the electronic structure of the substituted cation plays an important role.

2. Experimental

Polycrystalline samples of $CuFe_{1-x}Rh_xO_2$ were prepared from x=0.00 up to 0.10 by step of 0.02, and from x=0.15 to 0.25 by step of 0.05. Stoichiometric mixtures (1 g) of Cu_2O, Fe_2O_3 and Rh_2O_3 were ground and pressed in bars, which were set in alumina crucible and put in silica tube. After sealing under primary vacuum, the samples were fired at 1050 °C for 12 h. The X-ray powder diffraction patterns of the reacted bars were collected with a PANalytical diffractometer equipped with a Cu$K\alpha$ source ($K\alpha_1$ and $K\alpha_2$) in the 2θ range from 10° to 90° at room temperature. EDS (energy dispersive spectroscopy) analyses were performed by using a Zeiss Supra 55 scanning electronic microscope.

Magnetization dependence on temperature was measured in a Quantum Design superconducting quantum interference device (SQUID) magnetometer while warming from 2.5 to 50 K in 0.3 T (zero field cooling, ZFC). The dielectric and polarization measurements, and magnetization dependence on magnetic field were performed in a PPMS Quantum Design cryostat, the magnetization data from 0 to 14 T being collected with the ACMS option.

The samples for dielectric and polarization measurements were thin plates about 0.50 mm thick, and with a surface of approximately 5 mm^2. Silver paste was used to make electrical contacts. Dielectric permittivity was measured on heating with 1 K/min rate using an Agilent 4248A RLC bridge. Polarization was measured using an automatic pyroelectric current integration by a Keithley 6517A electrometer. The samples have been cooled from 20 to 5 K in a poling field of 450 kV/m. The electric field was removed and a waiting time of approximately 3600 s was applied to reach the polarization stability. Data were collected upon warming, or upon increasing the magnetic field.

3. Results

3.1. Structural characterizations

For studied x range (from 0.00 to 0.25), the powder X-ray diffraction patterns show the existence of the delafossite phase with the space group R-3m. The crystal structure consists of an alternative stacking along the c-axis (by using the hexagonal setting) of edge-shared $(Fe,Rh)O_6$ octahedra with the CdI_2-type structure separated by layers of Cu. The trivalent iron cations form a planar triangular network in the (a,b) plane (inset of Fig. 1).

In all samples, a small amount of impurities ($\leq$2% of iron oxides, Fe_3O_4 for x=0.00 or FeO for the substituted samples) was also detected. This observation is consistent with the presence of magnetic impurity in $CuFeO_2$ previously reported [23] for similar synthesis conditions. The obtained patterns were refined by Rietveld method using the Fullprof software [24]. A typical example is given for $CuFe_{0.92}Rh_{0.08}O_2$ (x=0.08) in Fig. 1. As shown in Fig. 2, the unit cell parameters exhibit little variations compared with pure $CuFeO_2$ [25], which is in good agreement with the closeness of the ionic radii between Fe^{3+} and Rh^{3+} in a six-fold coordination (r^{3+}_{Fe}=0.645 Å; r^{3+}_{Rh}=0.665 Å [26]). The only observable variation is the monotonous c increase with x from 17.1688(4) Å for x=0.02 to 17.1868(4) Å for x=0.15. Such a structural behavior is consistent with the small difference of the ionic radii which makes possible the formation of the solid solution while keeping the delafossite structure [27]. The EDS analyses, performed on each sample, confirm that the actual

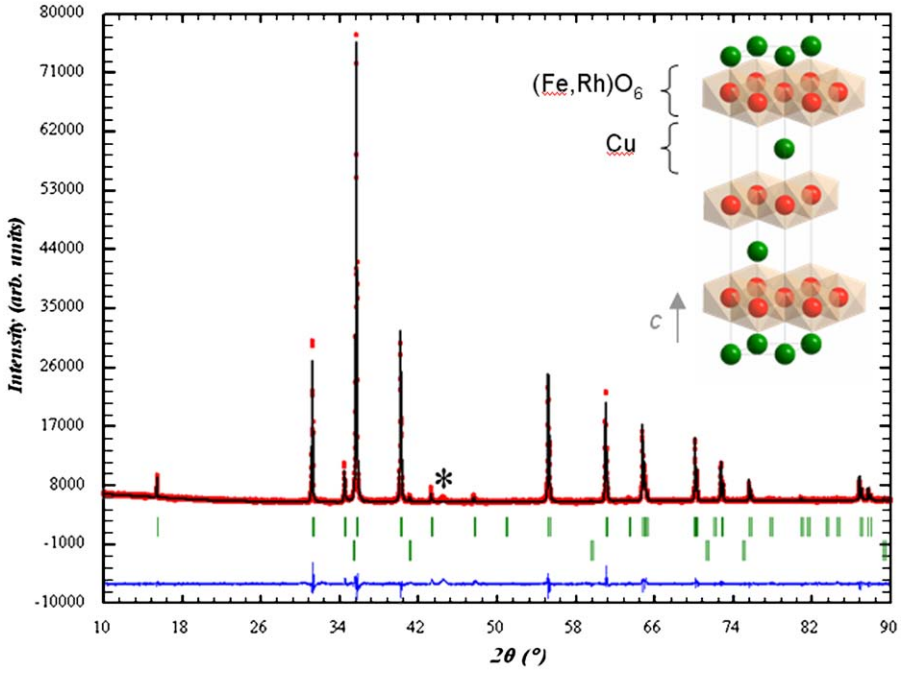

Fig. 1. Experimental X-ray powder diffraction pattern (red points) and calculated pattern (black line) of $CuFe_{0.92}Rh_{0.08}O_2$. The difference is given as a bottom line. The first set of Bragg ticks corresponds to the R-3m space group of the delafossite, the second one is for FeO (≅ 1% in weight), and the broad peak at 44° (*) comes from the sample holder. Inset: Schematic drawing of the $CuFe_{1-x}Rh_xO_2$ delafossite structure showing the network of edge-shared $(Fe,Rh)O_6$ octahedra separated by layers of Cu. (For interpretation of the references to color in this figure legend, the reader is referred to the web version of this article.)

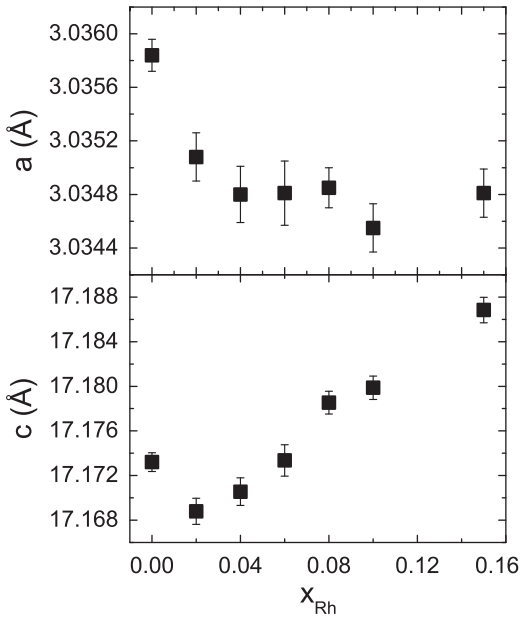

Fig. 2. a and c refined cell parameters of $CuFe_{1-x}Rh_xO_2$ as a function of the Rh content (x_{Rh}). For the x=0.00 composition, the presence of Fe_3O_4 might explain the shift of the a and c unit cell parameters.

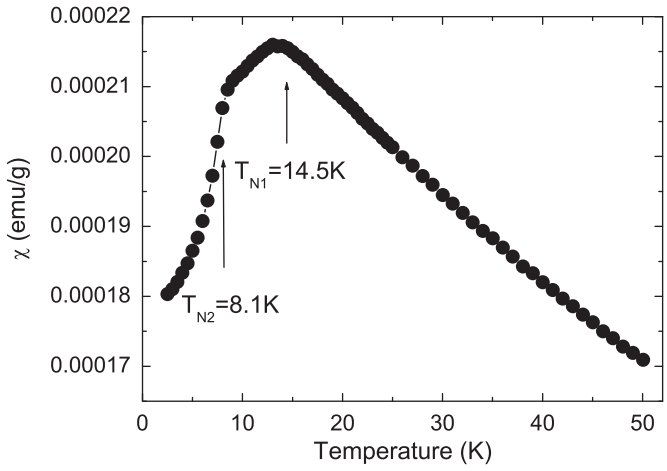

Fig. 3. ZFC (0.3 T) magnetic susceptibility of $CuFe_{0.92}Rh_{0.08}O_2$ as a function of temperature measured on heating.

composition corresponds to the nominal one (in the accuracy of the technique). According to the coexistence of three different mixed-valency metals which preclude the use of iodometric titration, refinements from neutron diffraction data are the only tool to determine accurately the oxygen content in this system. However, all the samples being prepared in the same conditions (O_2 starting stoichiometry, amount of powder, evacuated ampoule), their oxygen content is assumed to be the same, i.e. close to 2. Moreover, this assumption is supported by a previous study of $CuFeO_2$ showing that this compound does not accommodate large oxygen off-stoichiometry [28].

3.2. Physical properties

In order to probe the effect of the rhodium substitution upon the magnetic transition of $CuFeO_2$, T-dependent magnetization curves have been collected for all the samples. The antiferromagnetic transitions in $CuFeO_2$, from paramagnetic to collinear incommensurate ($T_{N1} \cong 14$ K) and then collinear commensurate below $T_{N2} \cong 11$ K [4] are known to be difficult to determine from the magnetic susceptibility $\chi(T)$ curves of polycrystalline samples. Our $\chi(T)$ curves, obtained from the magnetization ones, are illustrated in Fig. 3 for x=0.08. By decreasing T from the paramagnetic region, the curves are characterized by a rather broad maximum followed by a more abrupt transition. The temperature of the χ maximum corresponds to T_{N1} ($\cong$ 14.5 K) and the second transition, corresponding to an abrupt decrease of the magnetic susceptibility, at $\cong$ 8.1 K, can be associated to T_{N2}. The latter has to be compared to the value found for the undoped compound [29] ($\cong$ 10.5 K), whereas T_{N1} is found to be rather independent on x. This is illustrated in Fig. 4 from the comparison of the normalized $\chi(T)$ curves: the Rh for Fe substitution in $CuFe_{1-x}Rh_xO_2$ makes T_{N2} decreasing but T_{N1} remains almost unchanged. The T_{N2} and T_{N1} values, summarized in Fig. 5, reveal a rather monotonous T_{N2} decrease as x increases, from T_{N2}=11.5 K down to T_{N2}=5.9 K for x=0.00 and 0.15, respectively. Such an evolution with x is much smoother than with Al^{3+} doping since as soon as $x > 0.03$ in $CuFe_{1-x}Al_xO_2$, T_{N2} becomes lower than 2 K [5].

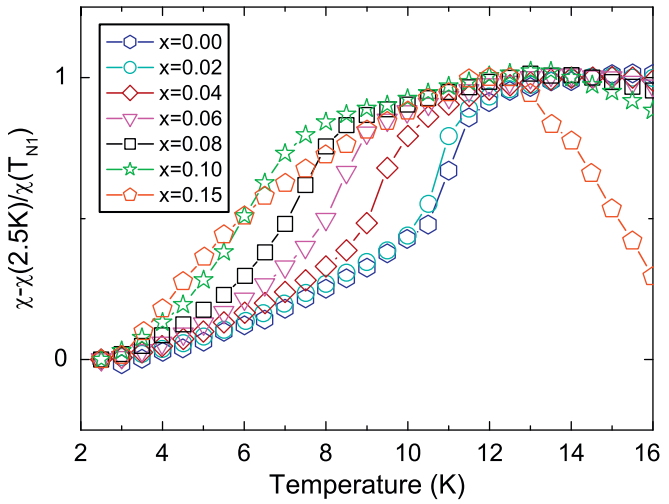

Fig. 4. Normalized magnetic susceptibility for the series $CuFe_{1-x}Rh_xO_2$.

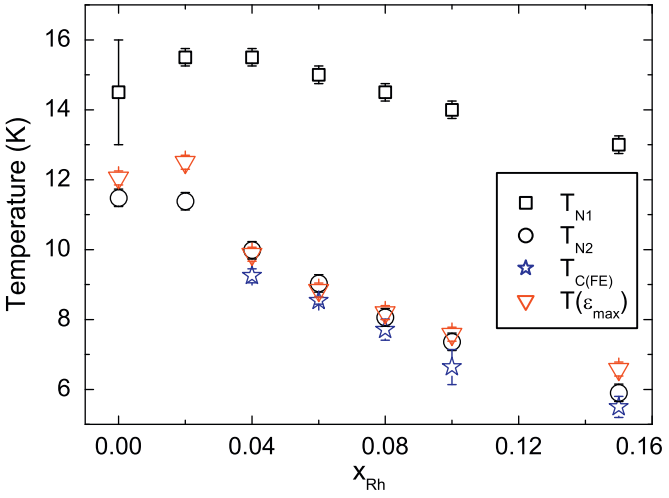

Fig. 5. Variation of the characteristic antiferromagnetic ordering temperatures (T_{N1} and T_{N2}), ferroelectric Curie temperature ($T_{C(FE)}$) and temperature of the peak in the dielectric constant ($T(\varepsilon_{max})$) as a function of the rhodium substitution (x_{Rh}).

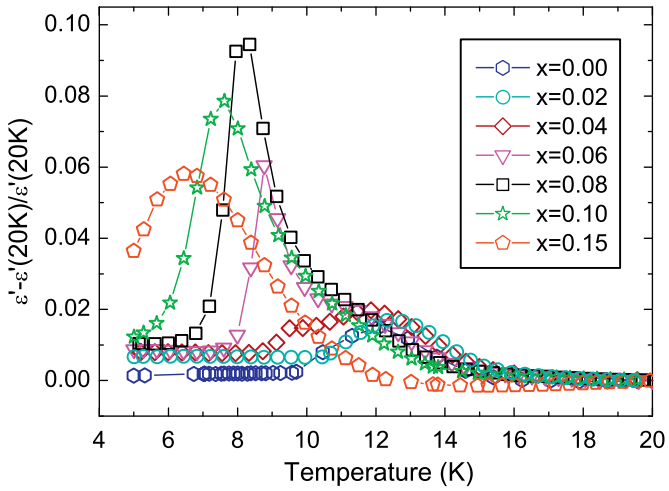

Fig. 6. Relative dielectric permittivity as a function of temperature, measured at 100 kHz while heating.

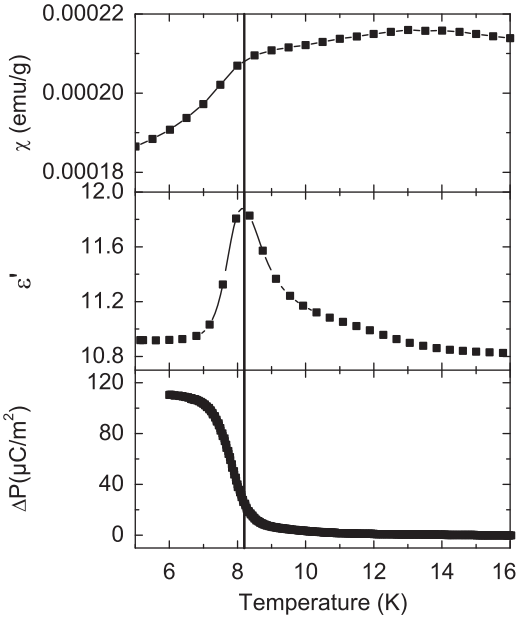

Fig. 7. Magnetic susceptibility, dielectric permittivity (100 kHz) and electric polarization (from up to down panels) of $CuFe_{0.92}Rh_{0.08}O_2$ measured upon warming.

As for $CuFeO_2$, the T-dependence of the dielectric permittivity (ε) of the $CuFe_{1-x}Rh_xO_2$ samples, recorded also upon warming, reveals a relationship between T_{N2} and ε (Figs. 5 and 6). For the $\varepsilon(T)$ curves, starting from $T > T_{N1}$, as T decreases, first ε starts to increase below T_{N1}, reaches a maximum value and then decreases. The temperature of the frequency independent ε maximum is in good coincidence with T_{N2} as shown in Fig. 7 for $CuFe_{0.92}Rh_{0.08}O_2$ (x=0.08). The dielectric losses are found to be order of 10^{-2} (or less) in the considered temperature range for all samples. It must be emphasized that the variation of the dielectric constant $\Delta\varepsilon$ with T is found to increase as x increases up to 8%, going from $\Delta\varepsilon/\varepsilon(20\,K)=0.02$ to $\Delta\varepsilon/\varepsilon(20\,K)=0.09$ as x goes from x=0.00 to 0.08. Beyond this optimal Rh concentration, the trend with x is opposite, $\Delta\varepsilon$ decreasing as x increases to reach $\Delta\varepsilon \cong 0$ for all Rh contents such as $x > 0.15$ (not shown) (Fig. 6).

As shown previously in $ACrO_2$ multiferroics [14], the larger variation of the dielectric constant comes with the larger electric polarization P according to the relation $\varepsilon - \varepsilon_\infty \propto \langle |\Delta P|^2 \rangle / k_B T$. This is confirmed along the series $CuFe_{1-x}Rh_xO_2$, as shown in Fig. 8a, by the $P(T)$ curves collected in the absence of magnetic field. In order to compare the electric change for all compositions, the same electric field cooling process, described in the experimental part, has been applied. Starting from the low levels of substitution characterized by P values close to 0, the P maximum value increases with x up to 110 μC m^{-2} for 8%-Rh and then P decreases being almost 0 (maximum of 10.5 μC m^{-2} at 5 K) for x=0.15. Clearly, it is found that P and ε magnitudes are connected as

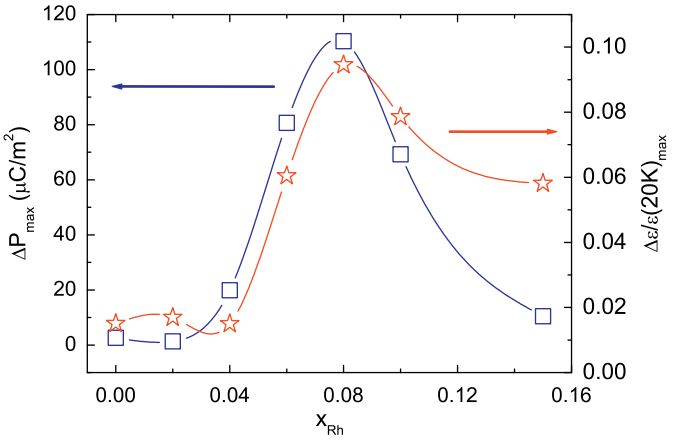

Fig. 9. Maximum of the electric polarization (left scale) and relative magnitude of the dielectric peak (right scale) as a function of Rh substitution.

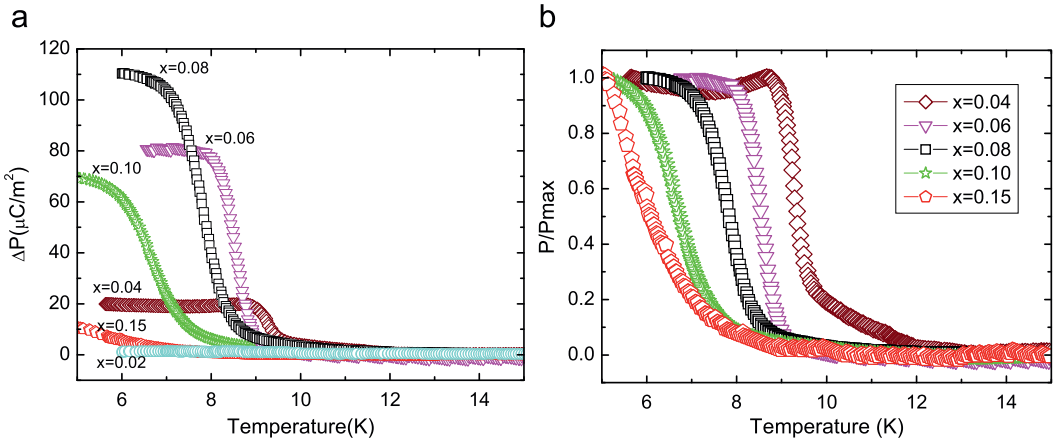

Fig. 8. (a) Electric polarization as a function of temperature for the series $CuFe_{1-x}Rh_xO_2$; (b) relative electric polarization as a function of temperature.

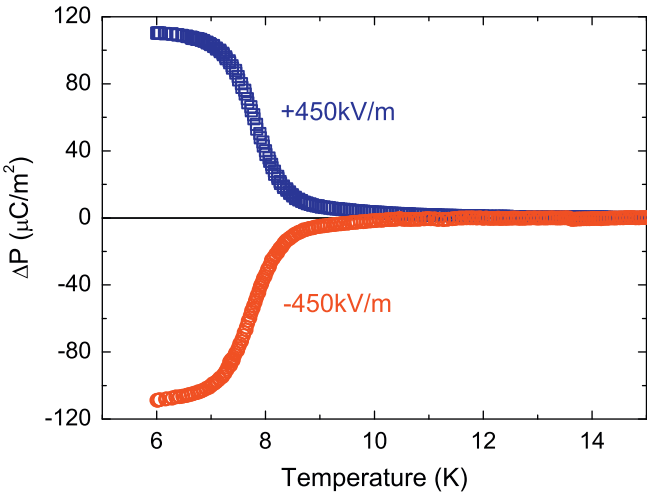

Fig. 10. Polarization reversal induced by sign change of the electric field ($E = \pm 450$ kV/m) for x=0.08.

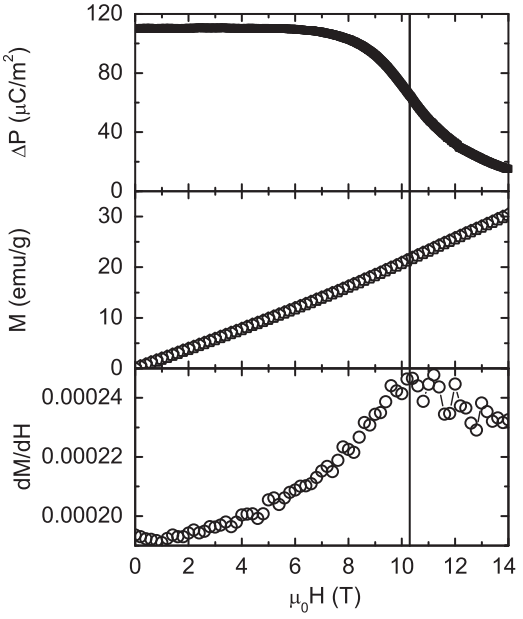

Fig. 11. Magnetic field dependence of polarization, magnetization and derivative curve dM/dH for $CuFe_{0.92}Rh_{0.08}O_2$ measured at 6 K.

illustrated in Fig. 9 by the comparison between the $P_{max}(x)$ and $\varepsilon_{max}(x)$ curves. Furthermore, the ferroelectric Curie temperatures ($T_{C(FE)}$) taken as the inflection point on the normalized curves of Fig. 8b and ε_{max} temperatures as a function of x are found also to correspond (Figs. 5 and 7 for x=0.08). The ferroelectric nature of the sample is also confirmed by the P reversal induced by the sign change of the electric field (Fig. 10 for x=0.08). Even if only ferroelectric loop measurements or 180° ferroelectric domains observation are proofs of ferroelectric property [30], such a loop was previously evidenced for $CuFe_{0.95}Rh_{0.05}O_2$ [12].

To give more direct evidence for magnetoelectric effect, the magnetic field H dependence of P has also been measured for x=0.08. The results for T=6 K (Fig. 11) demonstrate that above a critical H value, P tends to be suppressed. The corresponding critical magnetic field corresponds to a change of slope of the $M(H)$ curve (middle part of Fig. 11), as seen in the dM/dH curve (bottom part of Fig. 11).

4. Discussions

The present results obtained for polycrystalline $CuFe_{1-x}Rh_xO_2$ samples ($0.00 \le x \le 0.15$) confirm our first study of $CuFe_{0.95}Rh_{0.05}O_2$. This substitution stabilizes ferroelectricity for a broader range of substitution ($0.02 < x \le 0.15$) than in the case of the Al-substituted $CuFe_{1-x}Al_xO_2$ ($0.014 \le x \le 0.03$). The comparison of the characteristic temperatures $T(\varepsilon_{max})$, T_{N2} and $T_{C(FE)}$ as a function of x allows to show that this extension of the ferroelectric compositions is related to the much slower T_{N2} decrease induced by the Rh substitution. In both series (Al and Rh), since this magnetic transition T_{N2} corresponds to the upper limit of the ferroelectric region, a "spin induced" origin for the ferroelectricity can be invoked. As a consequence, the ferroelectric region in the (x, T) phase diagram is significantly extended (Fig. 12).

For the Al-series, studied by neutron diffraction [16], the ferroelectric phase (FE) is ascribed to an incommensurate (IC) non-collinear antiferromagnetic phase labeled "FEIC". This IC magnetic phase is characterized by magnetic Bragg reflections at $(qq\frac{3}{2})$ and $(\frac{1}{2}-q\frac{1}{2}-q\frac{3}{2})$ with an incommensurate q value of ~0.207 [5]. Such an incommensurate structure is related to the four-sublattice (4SL) commensurate magnetic structure of $CuFeO_2$ with $q=(\frac{1}{4}\frac{1}{4}\frac{3}{2})$. In fact, the Al effect can be compared to that of magnetic field H as the FEIC phase is induced by either substitution or external H application. The major difference between these perturbations acting on the spins is that for $CuFeO_2$, there exists a maximum magnetic field beyond which the FEIC phase transforms into a paraelectric ($qq0$) commensurate AF phase with $q=\frac{1}{5}$. It might be anticipated that Al substitution at random on the Fe network, though inducing FE, would not favor the stabilization of this magnetic field induced commensurate $\frac{1}{5}$ magnetic structure. In the present study, the existence of the FE state even for large Rh contents strongly suggests that the induced local disordering favors the incommensurable antiferromagnetic structure (FEIC) to which FE is associated.

Close behaviors are reported for Al and Ga substitutions, both trivalent cations being non-magnetic. The higher T_{N2} observed for x=0.037 in the Ga series compared to the same x in the Al-one is attributed to a smaller induced disorder due to closer cationic size of Ga^{3+} and Fe^{3+}. This size effect is in agreement with what is observed for Rh^{3+} whose the smoother impact on T_{N2} can be understood by considering the more extended 4d orbitals which should ensure a stronger hybridization with the oxygen orbitals even though Rh^{3+} adopts a t_{2g}^6 (S=0) low spin state in the

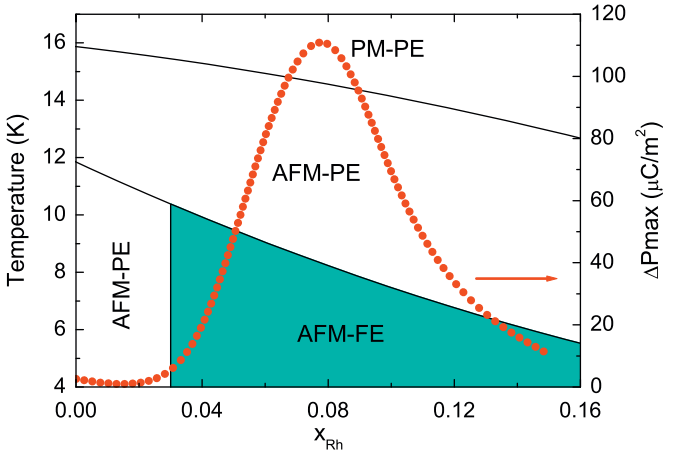

Fig. 12. Magnetic and electric (x, T) phase diagram for the series $CuFe_{1-x}Rh_xO_2$. The colored area corresponds to the ferroelectric region (AFM: antiferromagnetic; PM: paramagnetic; FE: ferroelectric; PE: paraelectric). Right y-axis: maximum of the electric polarization.

delafossite structure $CuRhO_2$ [10]. However, the suppression of the polarization by applied magnetic field for $CuFe_{0.92}Rh_{0.08}O_2$ indicates that a magnetic field induced transition from the FEIC state to a non-polar state also exists in the Rh doped $CuFeO_2$. For the Al doped phase, the FE vanishing for $x \geq 0.035$ was ascribed to a change of magnetic structure, i.e. oblique partially disordered phase (OPD). A similar magnetic phase could also be at the origin of the non-polar state for $x > 0.15$ in the $CuFe_{1-x}Rh_xO_2$ series.

As the samples of the present study are ceramics, it is not possible to address definitively the existence of an optimal composition with largest values of both P and ε. However, as a clear trend is observed, one might expect some subtle changes in the IC antiferromagnetic structure responsible for such an optimization. Finally, the $CuFe_{1-x}Rh_xO_2$ compounds, which offer a broad composition range with FEIC state, might help in understanding microscopic models proposed so far to explain the spin induced ferroelectricity. As both spin–current and magnetostriction models cannot be used in the case of the multiferroic delafossites such as $CuFeO_2$ or $CuCrO_2$, an alternative model based on d–p orbital hybridization, between orbitals of Fe^{3+} magnetic cations and O^{2-} anions, which varies with the spin–orbit coupling has been proposed [31] and supported by a polarized neutron diffraction study [32]. In that respect, the ability of Rh^{3+} orbitals to hybridize with oxygen would be a crucial difference with Al^{3+} to explain the existence of the FEIC phase for a much broader range of substitution.

Acknowledgments

The authors acknowledge K. Singh for help during measurements. Financial support for this work was partially provided by the French Agence Nationale de la Recherche, Grant no ANR-08-BLAN-0005-01.

References

[1] See for instance references in "Metal–Insulator Transitions" by Nevill Mott, Ed. Taylor & Francis.
[2] B. Raveau, A. Maignan, C. Martin, J. Solid State Chem. 130 (1997) 162.
[3] F. Ye, Y. Ren, Q. Huang, J.A. Fernandez-Baca, P. Dai, J.W. Lynn, T. Kimura, Phys. Rev. B 73 (2006) 220404.
[4] T. Kimura, J.C. Lashley, A.P. Ramirez, Phys. Rev. B 73 (2006) 220401(R).
[5] N. Terada, S. Mitsuda, T. Fujii, K. Soejma, I. Doi, H.A. Katori, Y. Noda, J. Phys. Soc. Jpn. 74 (2005) 2604.
[6] S. Kanetsuki, S. Mitsuda, T. Nakajima, D. Anazawa, H.A. Katori, K. Prokes, J. Phys. Condens. Matter 19 (2007) 145244.
[7] S. Seki, Y. Yamasaki, Y. Shiomi, S. Iguchi, Y. Onose, Y. Tokura, Phys. Rev. B 75 (2007) 100403(R).
[8] T. Nakajima, S. Mitsuda, S. Kanetsuki, K. Tanaka, K. Fujii, N. Terada, M. Soda, M. Matsuura, K. Hirota, Phys. Rev. B 77 (2008) 052401.
[9] N. Terada, S. Mitsuda, Y. Tanaka, Y. Tabata, K. Katsumata, A. Kikkawa, J. Phys. Soc. Jpn. 77 (2008) 054701.
[10] H. Kuriyama, M. Nohara, T. Sasagawa, K. Takubo, T. Mizokawa, K. Kimura, H. Takagi, in: Proceedings of International Conference on Thermoelectrics, 2006, p. 97.
[11] N. Terada, T. Nakajima, S. Mitsuda, H. Kitazawa, K. Kaneko, N. Metoki, Phys. Rev. B 78 (2008) 014101.
[12] B. Kundys, A. Maignan, D. Pelloquin, Ch. Simon, Solid State Sci. 11 (2009) 1035.
[13] N. Kida, Y. Ikebe, Y. Takahashi, J.P. He, Y. Kaneko, Y. Yamasaki, R. Shimano, T. Arima, N. Nagaosa, Y. Tokura, Phys. Rev. B 78 (2008) 104414.
[14] S. Seki, Y. Onose, Y. Tokura, Phys. Rev. Lett. 101 (2008) 067204.
[15] G. Lawes, A.B. Harris, T. Kimura, N. Rogado, R.J. Cava, A. Aharony, O. Entin-Wohlman, T. Yildirim, M. Kenzelmann, C. Broholm, A.P. Ramirez, Phys. Rev. Lett. 95 (2005) 087205.
[16] T. Nakajima, S. Mitsuda, S. Kanetsuki, K. Prokes, A. Podlesnyak, H. Kimura, Y. Noda, J. Phys. Soc. Jpn. 76 (2007) 043709.
[17] T. Kimura, G. Lawes, T. Goto, Y. Tokura, A.P. Ramirez, Phys. Rev. B 71 (2005) 224425.
[18] T. Kimura, T. Goto, H. Shintani, K. Ishizaka, T. Arima, Y. Tokura, Nature (London, UK) 426 (2003) 55.
[19] K. Taniguchi, N. Abe, T. Takenobu, Y. Iwasa, T. Arima, Phys. Rev. Lett. 97 (2006) 097203.
[20] K. Taniguchi, N. Abe, H. Sagayama, S. Ohtani, T. Takenobu, Y. Iwasa, T. Arima, Phys. Rev. B 77 (2008) 064408.
[21] A.H. Arkenbout, T.T.M. Palstra, T. Siegrist, T. Kimura, Phys. Rev. B 74 (2006) 184431.
[22] B. Kundys, A. Maignan, Ch. Simon, Appl. Phys. Lett. 94 (2009) 072506.
[23] J.P. Doumerc, A. Wichainchai, A. Ammar, M. Pouchard, P. Hagenmuller, Mater. Res. Bull. 21 (1986) 745.
[24] J. Rodriguez-Carvajal, Physica B 192 (1993) 55.
[25] A. Pabst, Am. Mineral. 23 (1938) 175.
[26] R.D. Shannon, Acta Crystallogr. A 32 (1976) 751.
[27] J.P. Doumerc, M. Pouchard, P. Hagenmuller, M. Elazhari, A. Ammar, M. Elaatmani, Mater. Res. Bull. 27 (1992) 39.
[28] E. Mugnier, A. Barnabé, P. Tailhades, Solid State Ionics 177 (2006) 607.
[29] S. Mitsuda, N. Kasahara, T. Uno, M. Mase, J. Phys. Soc. Jpn. 67 (1998) 4026.
[30] B. Jaffe, W.R. Cook, H. Jaffe, Piezoelectric Ceramics, Academic Press, New York, 1971.
[31] T. Arima, J. Phys. Soc. Jpn. 76 (2007) 073702.
[32] T. Nakajima, S. Mitsuda, K. Takahashi, M. Yamano, K. Masuda, H. Yamazaki, K. Prokes, K. Kiefer, S. Gerischer, N. Terada, H. Kitazawa, M. Matsuda, K. Kakurai, H. Kimura, Y. Noda, M. Soda, M. Matsuura, K. Hirota, Phys. Rev. B 79 (2009) 214423.